Modelling and simulation of switched reluctance motor drive

DEBIPRASAD PANDA AND V. RAMANARAYANAN
Department of Electrical Engineering, Indian Institute of Science, Bangalore 560 012, India.
emails: dpanda@ieee.org and vram@ee.iisc.ernet.in; Fax: 91(0)80 360 0444, 91(0)80 360 0683.

Abstract

Switched reluctance (SR) motor has a number of promising features like simplicity, ruggedness, reliability and cost-effectiveness. It offers relatively high torque-on-inertia ratio, is capable of running at high speeds and has high efficiency. In all, it has a good potential for motion-control applications. However, the need of a dedicated power converter, higher torque ripple and higher audible noise are its major limitations. In this paper, the constructional features of SR motor are briefly discussed. With experimentally obtained flux-linkage and static torque characteristics, a suitable model of the motor is achieved. Dynamic simulation of the motor using time-step integration method is discussed. Desired control parameters T_{ON}, T_{OFF} and I^*, for different speeds and torques are obtained through open loop simulation. The torque ripple for different combinations of the above parameters is illustrated. Closed loop dynamic performance is studied in simulation and results of current, torque, and speed waveforms are presented. The torque-speed envelope of the SR motor is found through simulation and the results for the same are presented.

Keywords: Switched reluctance motor, flux-linkage characteristics, speed control.

1. Introduction

Switched reluctance (SR) motor has a number of promising features. Professor Lawrenson in a seminal paper[1] in 1980 opened up its potential and inspired researchers to exploit the possibilities for variable speed applications. Besides its simplicity, it is quite rugged, reliable, and inexpensive too. It offers relatively high torque-to-inertia ratio, is capable of running at high speeds, and has high efficiency. In all, it has a good potential for motion control applications.

Though the mechanical construction of the motor is extremely simple, the flux-linkage characteristics and torque production mechanism are highly nonlinear,[2] which makes the analysis and controller design of the drive complex. Its major limitations are that line start is not possible, it needs a power converter and rotor position to start and run and generates high torque ripple and audiable noise. Mercifully, several control algorithms are available in the literature for torque ripple minimisation,[3] sensorless operation[4-7] and acoustic noise reduction.[8, 9]

In this paper, modelling and simulation of the SR motor is addressed. The flux and torque are nonlinear functions of phase current and rotor position. The controller design of such nonlinear systems requires computer-based modelling. Besides, the nonlinear equations gov-

erning its dynamics are difficult to solve analytically. Dynamic simulation is more convenient to study the performance of this drive.

The outline of this paper is as follows. Constructional features of the SR motor are briefly described followed by experimenatlly obtained flux-linkage and static torque characteristics. With the experimental data obtained a suitable model of the motor is achieved. Dynamic simulation of the motor using time-step integration is discussed. The desired control parameters, T_{ON}, T_{OFF} and I^*, for different speeds and torques are obtained through open loop simulation. The torque ripple for different combinations of the above parameters is illustrated. The torque and speed waveforms of the drive during steady state and transient are shown. The torque-speed envelope is found and its results are presented.

2. Construction

The construction of the SR motor is different from conventional motors. Unlike the conventional machines, the number of stator and rotor poles in SR motor is different. The most popularly used SR motors have stator : rotor pole numbers of 6 : 4 and 8 : 6. Other possible configurations are 6 : 2, 8 : 6, 10 : 4, 12 : 8.[10] Even 2 : 2 single-phase motors are possible, but they require extra parking magnet or some other starting mechanism.[10] Similarly, 3 : 2, 4 : 2 and many other configurations are possible. The motor comprises a single stack. Both the stator and rotor are constructed from laminations. An 8 : 6 pole configuration is taken up here to demonstrate the different constructional features of the SR motor (Fig. 1a). This motor has four phases. Each phase winding is split into two diametrically opposite stator poles. To maintain the clarity of the figure, only phase1 (Ph1-Ph1') is shown with winding. In SR motor, the phases are excited through a power converter. For illustration, one phase winding with switching devices and supply voltage is shown in Fig. 1b. Semiconductor switches (S1, S2) are on while the phase is excited. Diodes D1, D2 are required for demagnetisation. The other phases follow similar kind of switching arrangement. In relation to the SR motor the following observations can be made (Fig. 1):
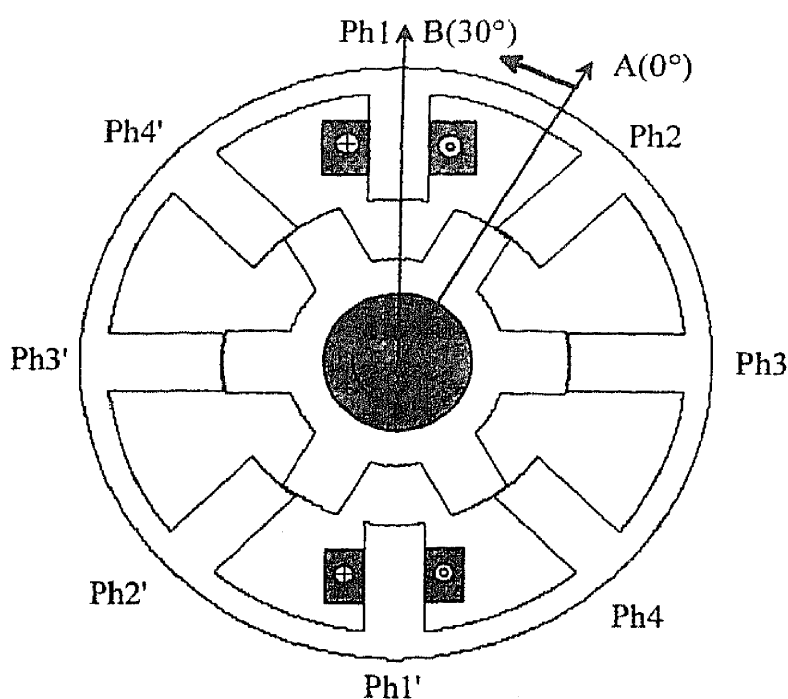

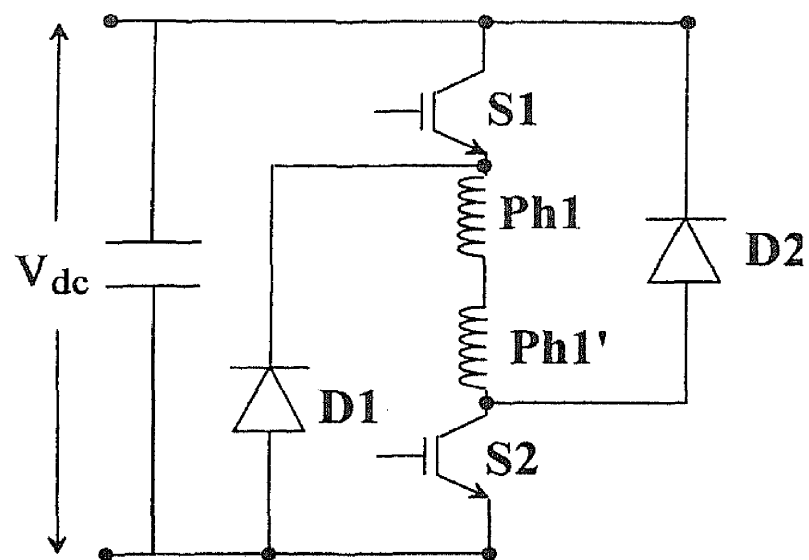FIG. 1a. Cross-section of an 8 : 6 pole four-phase SR motor.

FIG. 1b. Phase winding with switches.

- SR motor is doubly salient.
- Only stator is energised; the excitation voltage is purely DC.
- Stator winding is essentially of concentrated type.
- Rotor does not have any winding or permanent magnet.
- No carbon brush, commutator or slip ring is required, hence the motor is brushless.

The observations lead to the conclusion that the construction of the SR motor is simple. The absence of permanent magnets, carbon brushes, slip rings, commutators and cage bars makes this motor rugged and reliable. Such a rugged motor is quite suitable for very high-speed applications. Obviously, the manufacturing cost of this motor will be less.

3. Modelling

3.1. *Electrical subsystem*

The electromagnetic characteristics of the SR motor can be represented by the following equations.

$$v_j = R \times i_j + \frac{\mathrm{d}\psi_{jj}\left(\theta_j, i_j\right)}{\mathrm{d}t} + \sum_{\substack{k \neq j \\ k=1,2,3,4}} \frac{\mathrm{d}\psi_{jk}\left(\theta_k, i_k\right)}{\mathrm{d}t} \tag{1}$$

$$\psi_j = \psi_{jj} + \sum_{\substack{k \neq j \\ k=1,2,3,4}} \psi_{jk} \tag{2}$$

$$w'_j = \int \psi_j \mathrm{d}i_j \tag{3}$$

$$T_{ej} = \frac{\mathrm{d}w'_j}{\mathrm{d}\theta} \bigg|_{i_j} = \text{constant}, \tag{4}$$

where v_j is the phase voltage; i_j, ψ_{jj}, ψ_j, θ_j, W'_j and T_{ej}, respectively, are the current, self flux, net flux, position, coenergy and developed torque of jth phase, ψ_{jk} is the mutual flux linkage of jth phase due to other conducting phase (kth phase); i_k and θ_k are the current and position of kth phase. All the equations shown above are nonlinear and the solution of these equations is tedious. Using finite element method,[11] it is possible to solve these equations; however, the accuracy of these methods depends on the number of elements used for computation and physical understanding of the system. Besides, it is computationally complex. In this paper, an alternative modelling approach from test results is followed. The experimentally obtained data of static flux-linkage and static torque characteristics are used in modelling. Mutual flux and eddy current effects are neglected.

The experimental methods for measuring the flux-linkage and static torque characteristics of the motor are explained elsewhere (Figs 2a and b).[2] It may be seen that both the characteristics are nonlinear functions of position and current.

The static flux-linkage characteristics are approximated by the following mathematical expression.
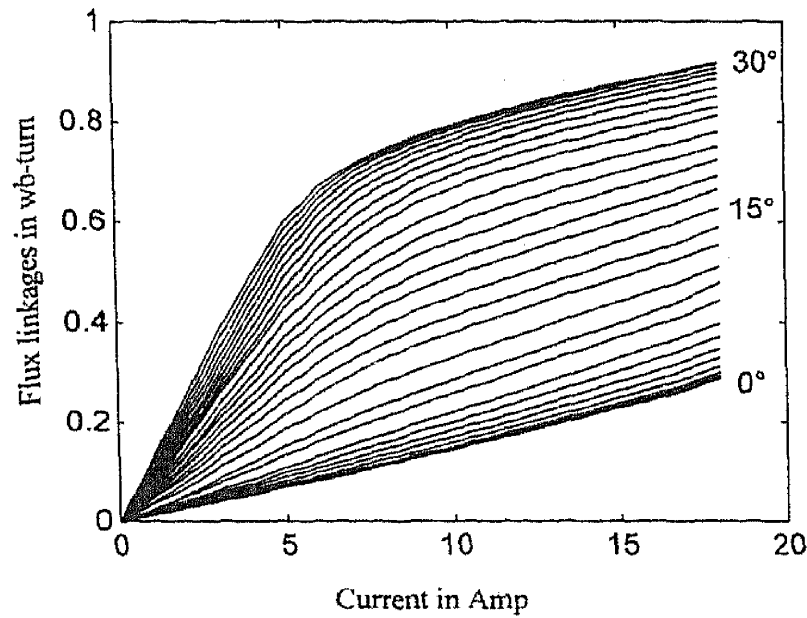
FIG. 2a. Experimentally obtained flux-linkage character-
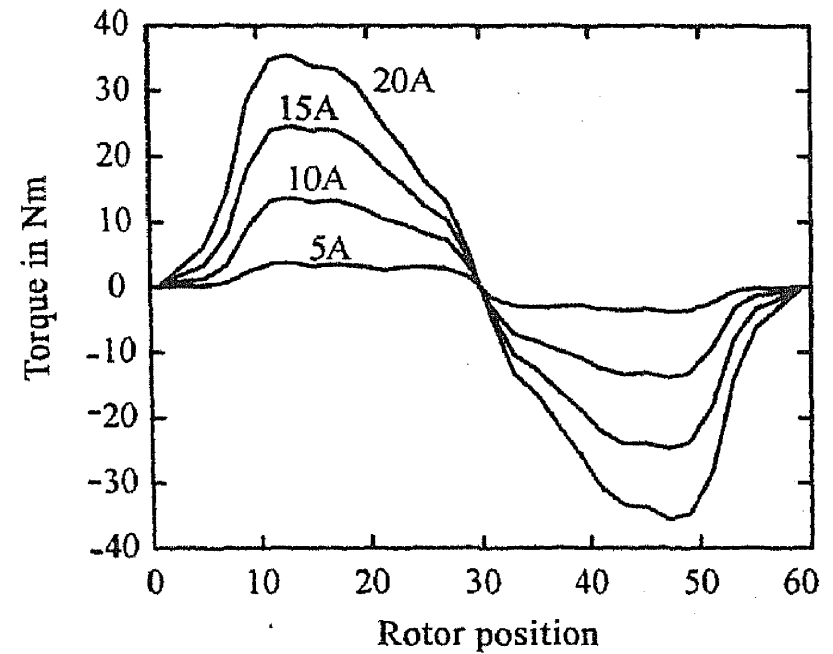istics for different positions (0° : 1° : 30°) and currents
(0 : 1 : 18 A).

FIG. 2b. Experimentally obtained static–torque charac-
teristics.

$$i = K_1(\theta)\,\Psi + m \times K_2 \times (\Psi - \Psi_1(\theta))^2 + n \times K_3(\Psi - \Psi_2(\theta))^3; \tag{5}$$

$$m = 1, \text{ if } \Psi > \Psi_1; \text{ otherwise } m = 0; \tag{5a}$$

$$n = 1, \text{ if } \Psi > \Psi_2; \text{ otherwise } n = 0, \tag{5b}$$

where i and ψ are the current and the flux linkage of a particular phase; K_2 and K_3 are constants and $K_1(\theta)$, $\psi_1(\theta)$, $\psi_2(\theta)$ are functions of position. For the test motor, the constants K_2 and K_3 are chosen as 11 and 185, respectively. The magnetic characteristics of a particular phase in SR motor are symmetric with respect to its aligned position (30° in this case). Hence, the need of modelling for the test motor is effectively reduced to a zone spanning from 0° to 30°. The above parameters $K_1(\theta)$, $\psi_1(\theta)$, $\psi_2(\theta)$ are stored in a look-up table for every 3°. Linear interpolation is used for intermediate values (Table I). To testify the accuracy of the above modelling, the test data and the curve following the mathematical expression in eqn (5) are plotted in Figs 3a–c for positions 0°, 15° and 30°, respectively.

Table I
Model parameters for the $\psi - i$ characteristics

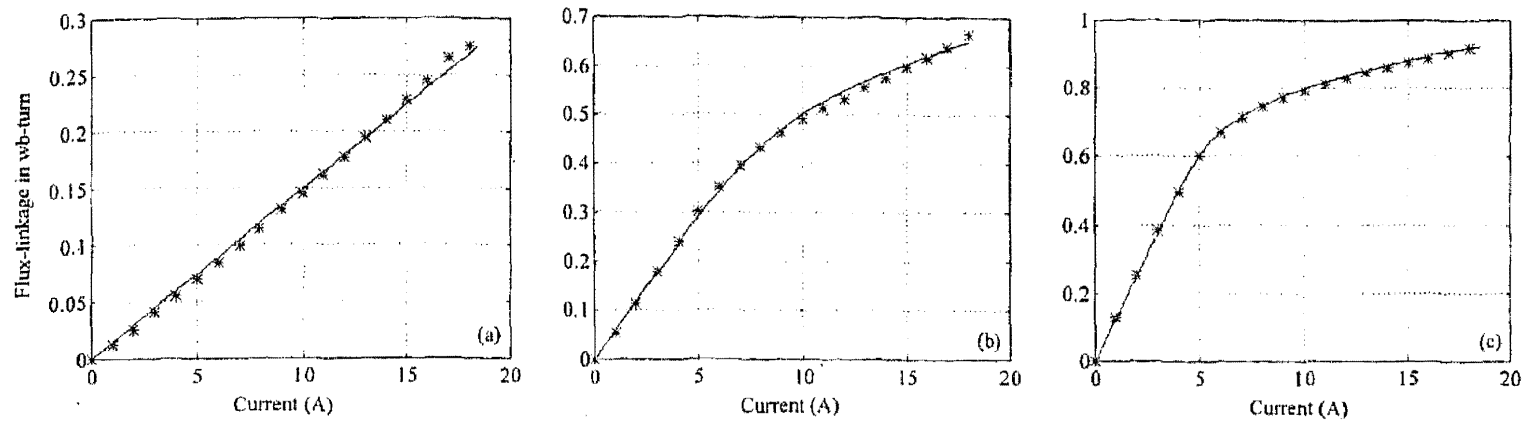| Position (θ)	$K1$	Ψ_1	Ψ_2
0°	67	0.25	0.25
3°	62.5	0.25	0.25
6°	53.5	0.25	0.25
9°	38	0.175	0.25
12°	23.5	0.2	0.275
15°	17	0.225	0.35
18°	14	0.335	0.43
21°	12	0.46	0.495
24°	10	0.47	0.545
27°	8.75	0.485	0.56
30°	8	0.485	0.56

FIG. 3. Comparsion of experimental data (***) and fit curve (continuous line) at (a) 0°, (b) 5° and (c) 30° positions.

3.2. Mechanical subsystem

In the present test set-up, a DC generator is used for loading the SR motor. Hence, the motor combined with the load completes the mechanical subsystem. For modelling the mechanical subsystem, frictional coefficient (B) and inertia (J) are required. B is obtained through no-load test.

The motor is run in no load at different speeds and the no-load torque at various speeds is noted with a torque transducer. B may be obtained by dividing the no-load torque by the speed of the motor. It is seen that the value of B varies with the speed. The average value of B obtained following the above process is 0.0065 Nm/rad/s.

The inertia of the system (load + SR motor) is obtained by retardation test. Figure 4 shows the speed versus time plot during the retardation test. The rated speed of the motor is 1500 rpm. From the plot it can be seen that the time taken for the speed to fall from 1500 to 500 rpm is about 12.25 s, which can be treated as the mechanical time constant (τ) of the total system. The inertia of the system can be computed using the expression, $J = \tau \times B$. Form the given value of $B = 0.0065$ Nm/rad/s, J is 0.08 kgm^2.

4. Simulation

4.1. Methodology and simulation block diagram

The basic algorithm for simulating the operation of the SR motor, followed in this work, is the time-stepping integration[2, 10] of the voltage equation:
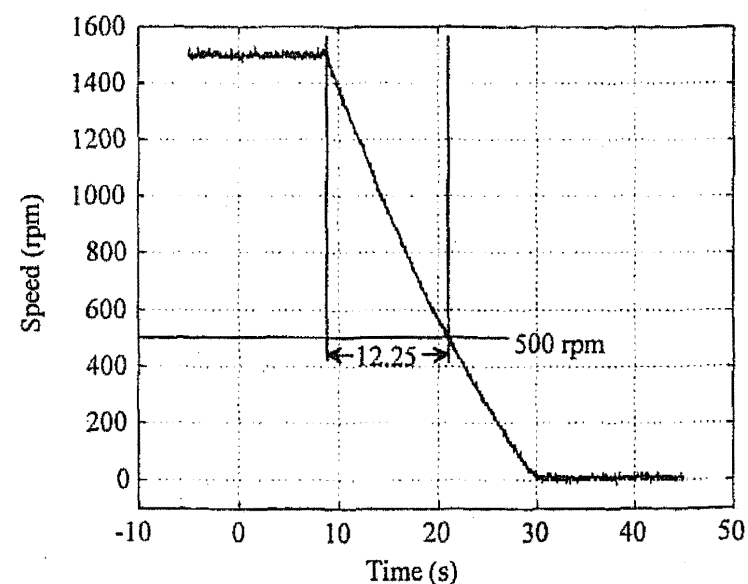

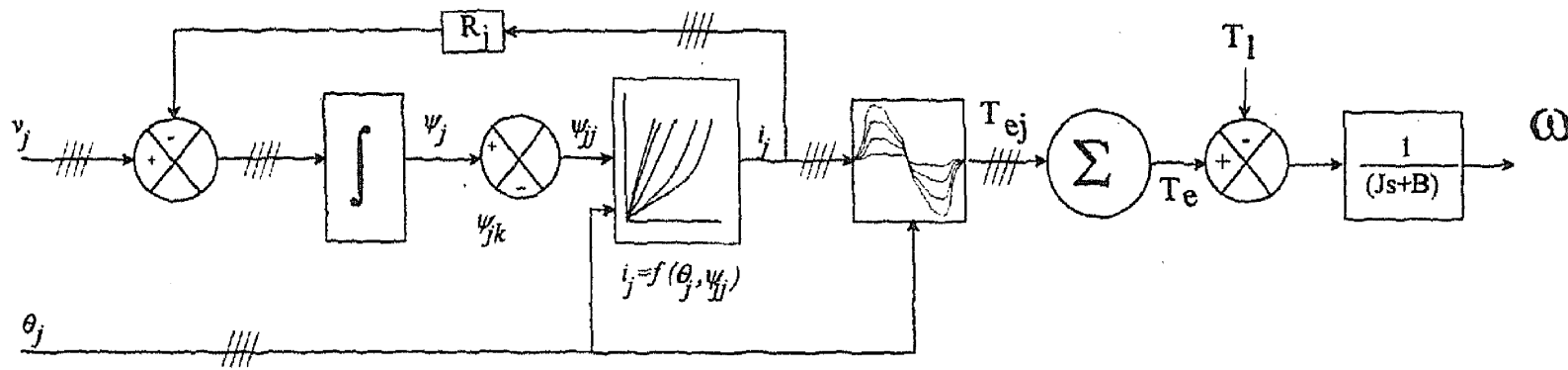FIG. 4. Speed vs time plot during retardation test of the SR motor (including the DC generator).

FIG. 5. Simulation block diagram of the SR motor.

$$\Psi_j = \int (v_j - R_j i_j) dt \qquad (6)$$

where v_j is the voltage applied to the phase winding, i_j the phase current and R_j the phase resistance. The phase voltage is a function of the DC supply voltage and the states of the switches in the controller. At any instant, the phase-flux linkage Ψ_j is obtained by integrating eqn (6) over the previous time step. Now with a known position (θ_j), the value of (i_j) may be found using the mathematical expression in eqn (5).

Once the value of current and the position of a particular phase is known, the instantaneous torque due to that particular phase may be found using the stored static torque data, $T_{ej} = f(i_j, \theta_j)$. Adopting a similar process, the torque due to other conducting phases also may be found. The summation of all the phase torques at any instant gives the instantaneous torque of the motor. The average torque over an electrical cycle can be obtained by summing and averaging the instantaneous torque over a period of 60° rotation. Alternatively, average torque may be computed through coenergy principle.[2, 10]

The instantaneous torque, T_e can be used to simulate the mechanical subsystem of the drive given by the following equation

$$T_e - T_1 = J \frac{d\Omega}{dt} + B\Omega \qquad (7)$$

where T_1 is the load torque, J the total inertia of the load and the motor and B the frictional coefficient of the total mechanical system. Speed is the output of the mechanical subsystem in the simulation. The same may be used to carry out the simulation with closed loop controllers. It will be discussed later in detail.

Adopting the above method, the dynamic and steady-state performance of the drive are studied through simulation. The basic simulation block diagram of the SR motor is shown in Fig. 5. Simulation is conducted with the following assumptions:

(i)   DC bus voltage is considered ripple free.

(ii) Eddy current effects are ignored.

(iii) Mutual fluxes are ignored.

(iv) Maximum switching frequency of the converter switches is limited to 10 kHz.

4.2. *Control parameter selection*

The control of the SR motor is largely divided into two regions: (i) low-speed chopping control and (ii) high-speed angle control. In the former, the T_{ON} and T_{OFF} angles are kept fixed and
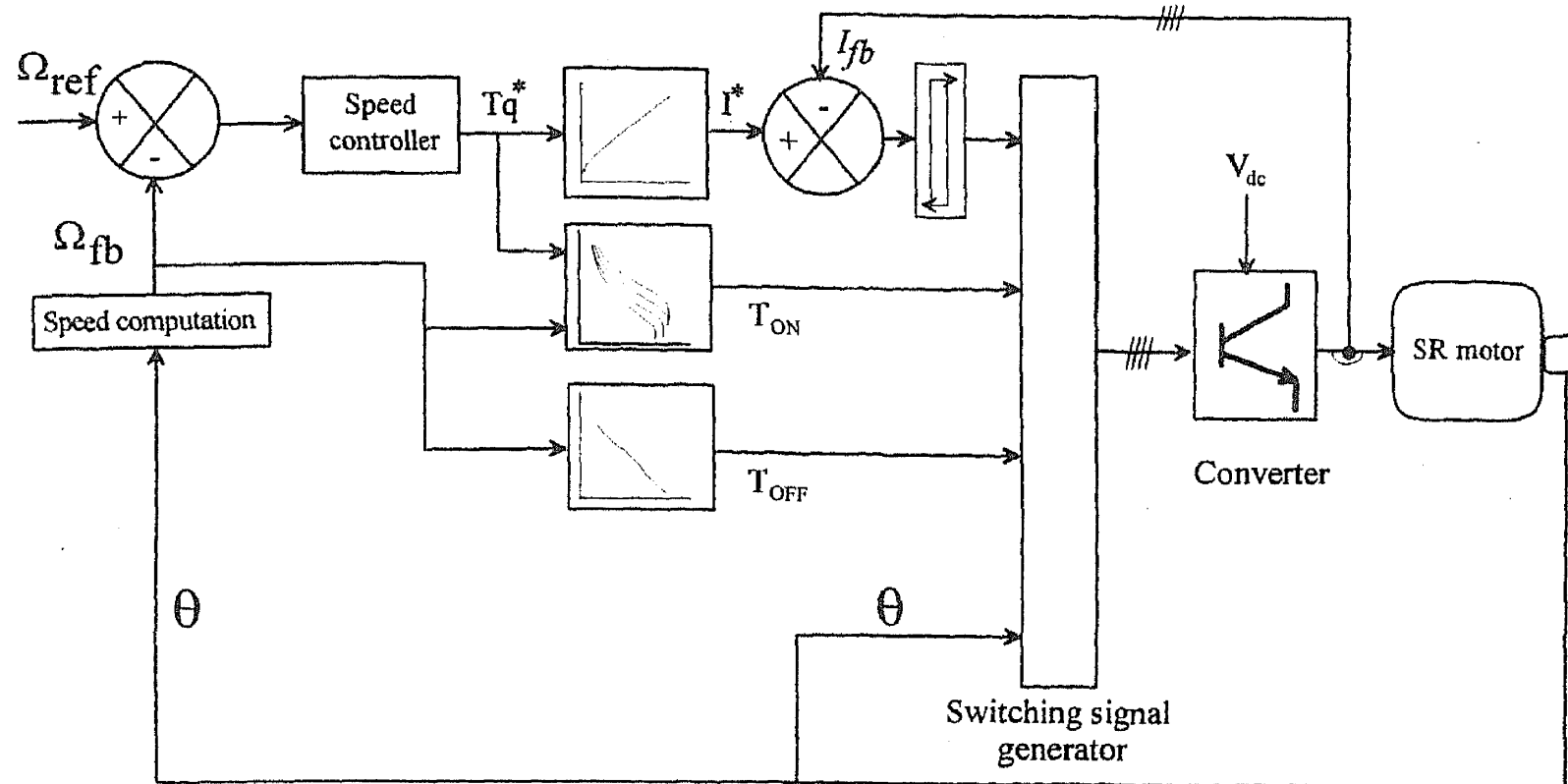
FIG. 6. Controller block diagram with estimator.

torque is controlled by regulating the current through winding. Normally, a hysteresis control or fixed frequency chopping control is used as current controller. On the other hand, in high-speed operation, back-emf is sufficiently high and chopping control is no longer possible. Thus the torque is controlled solely by the control of T_{ON} and T_{OFF} angles. The low-speed chopping control and high-speed angle control are illustrated in Fig. 6. The raw enable signal is the maximum duration for which a particular phase may be excited. The envelope of raw enable signal is strictly a function of speed of the machine. In low-speed chopping control, the phase current is maintained to its reference value by a hysteresis controller. The switching of a particular phase is restricted within the envelope of the raw enable signal as illustrated in Fig. 6. Thus, in this speed range, the T_{ON} and T_{OFF} angles are fixed for a given speed but current reference (I^*) is chosen as a function of load. On the other hand, in high-speed angle control mode the torque ripple is controlled by changing only the T_{ON} angle though the raw enable signal is chosen as a function of speed. Thus, the major control parameters for the whole speed range are represented as reference current (I^*), turn-on (T_{ON}) and turn-off (T_{OFF}) angles. The successful and efficient operation of an SR motor largely depends on the choice of these control parameters. The basic purpose of simulation is to choose the control parameters and study the performance of the drive prior to its actual implementation. The system is first simulated in
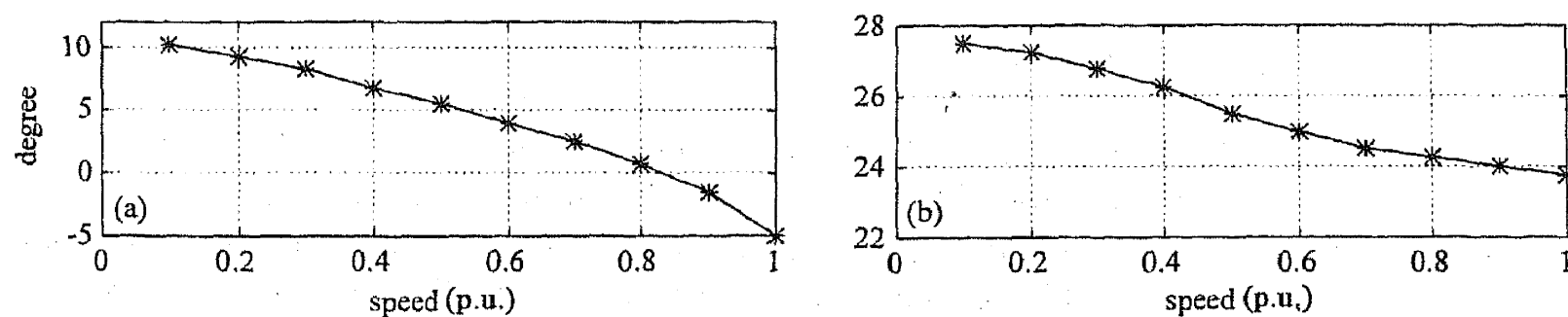
FIG. 7. An arbitrary set of T_{ON} and T_{OFF} angles for different speeds to obtain rated torque (25.5 Nm) with a peak current limit of 18 A. (a) T_{ON} vs speed and (b) T_{OFF} vs speed.
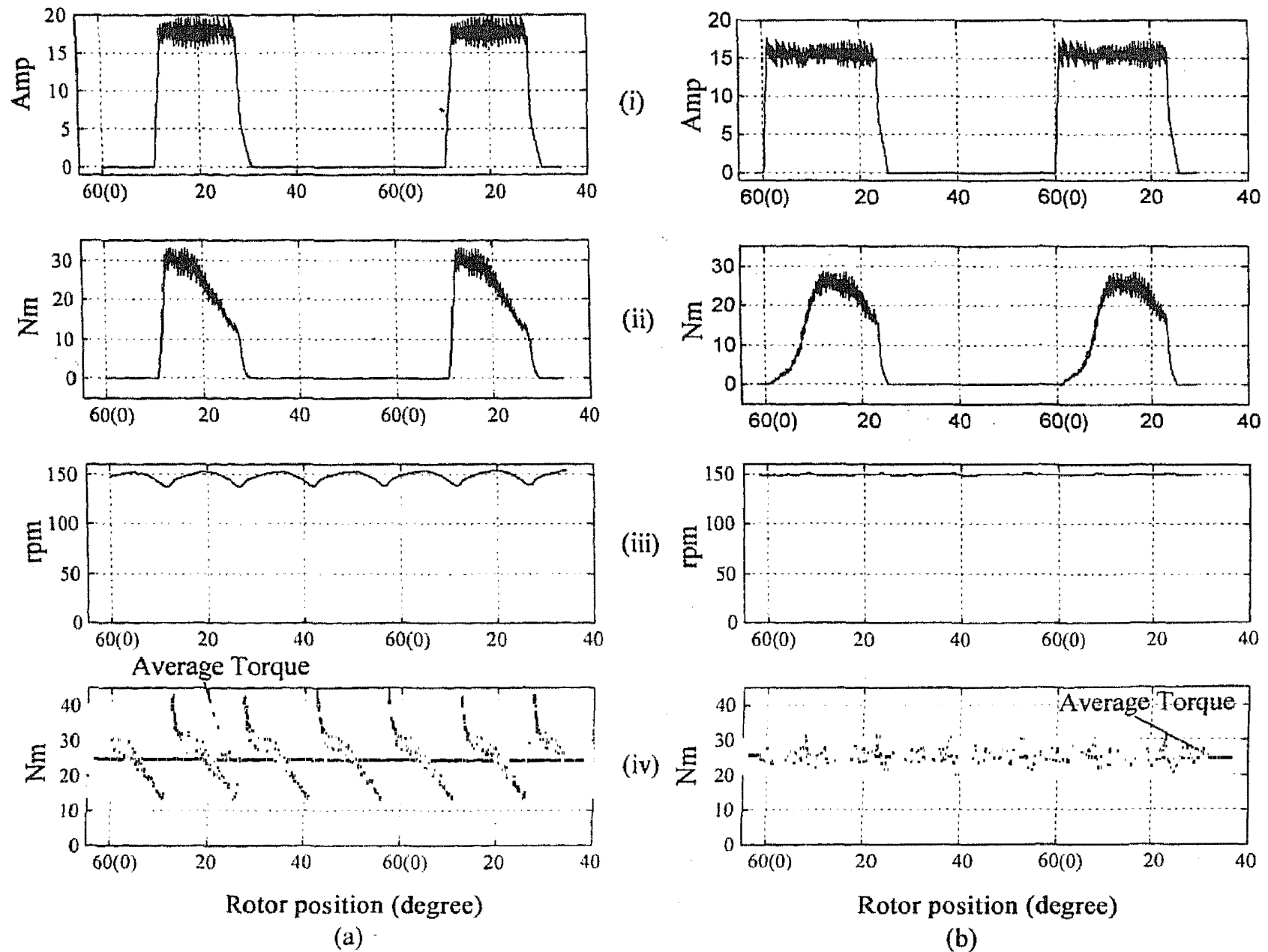
FIG. 8. Comparsion of simulation results of (i) phase current, (ii) phase torque, (iii) speed waveform, (iv) instantaneous and average torque at 150 rpm and full load for two cases, (a) with $T_{ON} = 10.5°$ and $T_{OFF} = 27.5°$ and (b) with $T_{ON} = 0°$ and $T_{OFF} = 23.15°$.

open-loop steady-state condition. It is assumed that the motor is running at a predetermined speed, and the required average torque is obtained by adjusting the T_{ON}, T_{OFF} and reference current I^*. It is observed that at any particular speed, the required average torque may be achieved by several combinations of parameters (Fig. 7). The combination which gives higher torque per peak current and lower torque ripple is desirable.

4.2.1. Illustration of torque ripple with different combinations of control parameters

A set of T_{ON} and T_{OFF} angles is arbitrarily chosen for different speeds and the rated torque is obtained with these values when the peak excitation current is limited to 18 A. The torque ripple in Fig. 8a, 9a and 10a is typical of these set of values. On the contrary, with a different set of the above parameters the torque ripple is reduced, though the average torque and speed are the same. Phase currents, phase torques, average torques and speeds with reduced torque ripple and different values of T_{ON} and T_{OFF} angles are given in Figs 8b, 9b and 10b. It may be concluded that by adjusting the T_{ON} and T_{OFF} angles, it is possible to bring down appreciably the torque ripple in low and medium speed ranges.
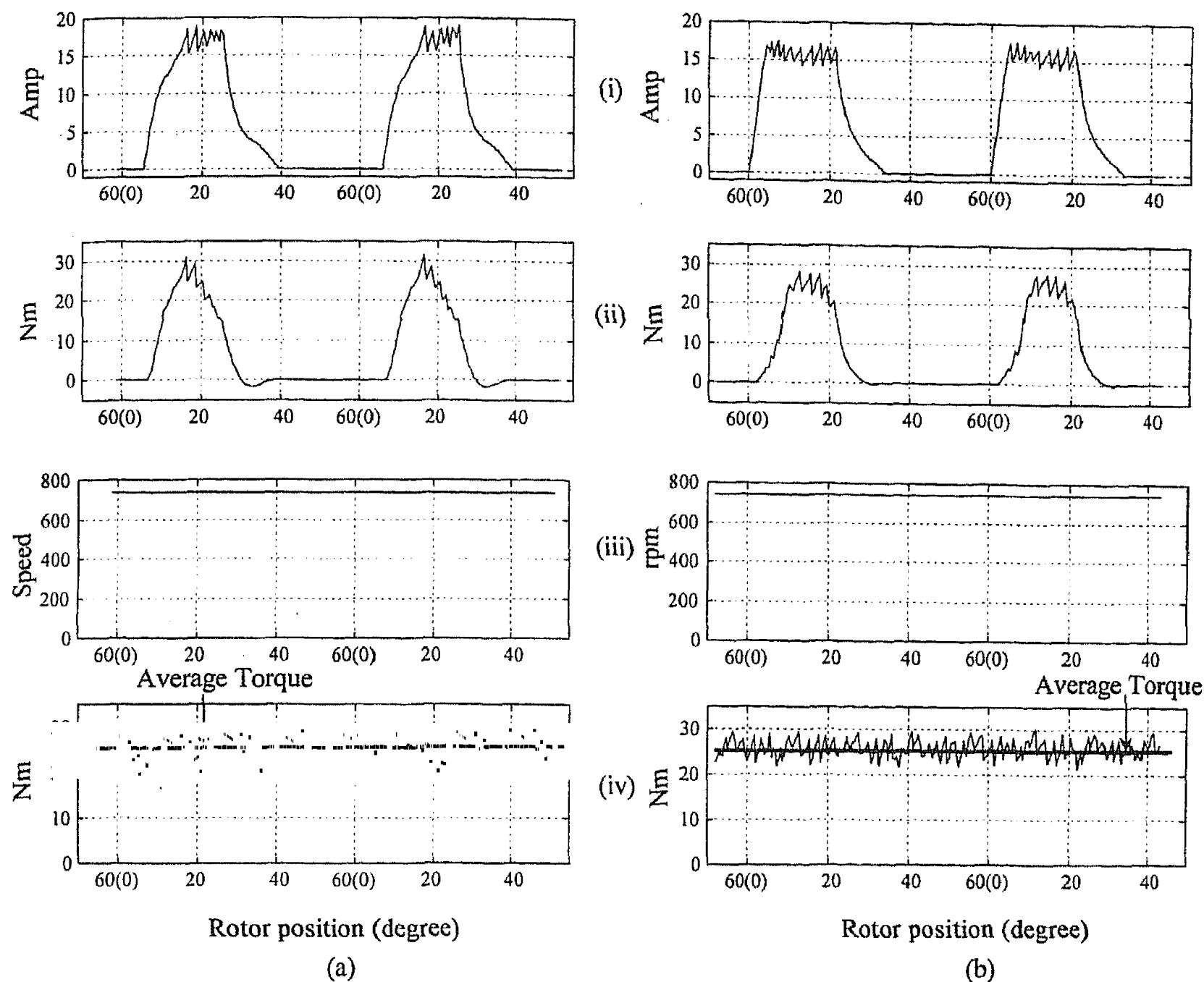
FIG. 9. Comparsion of simulation results of (i) phase current, (ii) phase torque, (iii) speed waveform and (iv) instantaneous and average torque at 750 rpm and full load (25.5 Nm) for two cases, (a) with $T_{ON} = 5.5°$ and $T_{OFF} = 25.5°$ and (b) with $T_{ON} = 0°$ and $T_{OFF} = 21.5°$

4.2.2. Final choice of parameters and closed loop simulation

A new set of T_{ON} and T_{OFF} angles is shown in Figs 11a and b. The duration between these is regarded as the raw enable signal for different speeds. Maximum torque is achieved for various speeds of the motor when the DC bus voltage is maintained at its rated value by choosing the T_{ON} and T_{OFF} angles as given in Figs 11a and b and with a current reference of 18 A (Fig. 12). At high speed, the T_{ON} angle is varied with both speed and demanded torque. Torque produced for different T_{ON} angles and speed are given in Fig. 13 when the T_{OFF} angles are maintained at the values as given in Fig. 11b. With overload condition, the T_{ON} angles may be further pushed towards the negative slope of inductance. For a peak current limit of 27 A (50% more than rated current, 18 A), torques along with corresponding T_{ON} angles for various speeds are plotted in Fig. 14. Thus the T_{ON} angle is varied with both speed and load. The set of values shown in Figs 11, 13 and 14 are used for controlling the test motor in the angle control mode up to the rated speed of the motor. The T_{OFF} angle is set as a function of speed (Fig. 11b).
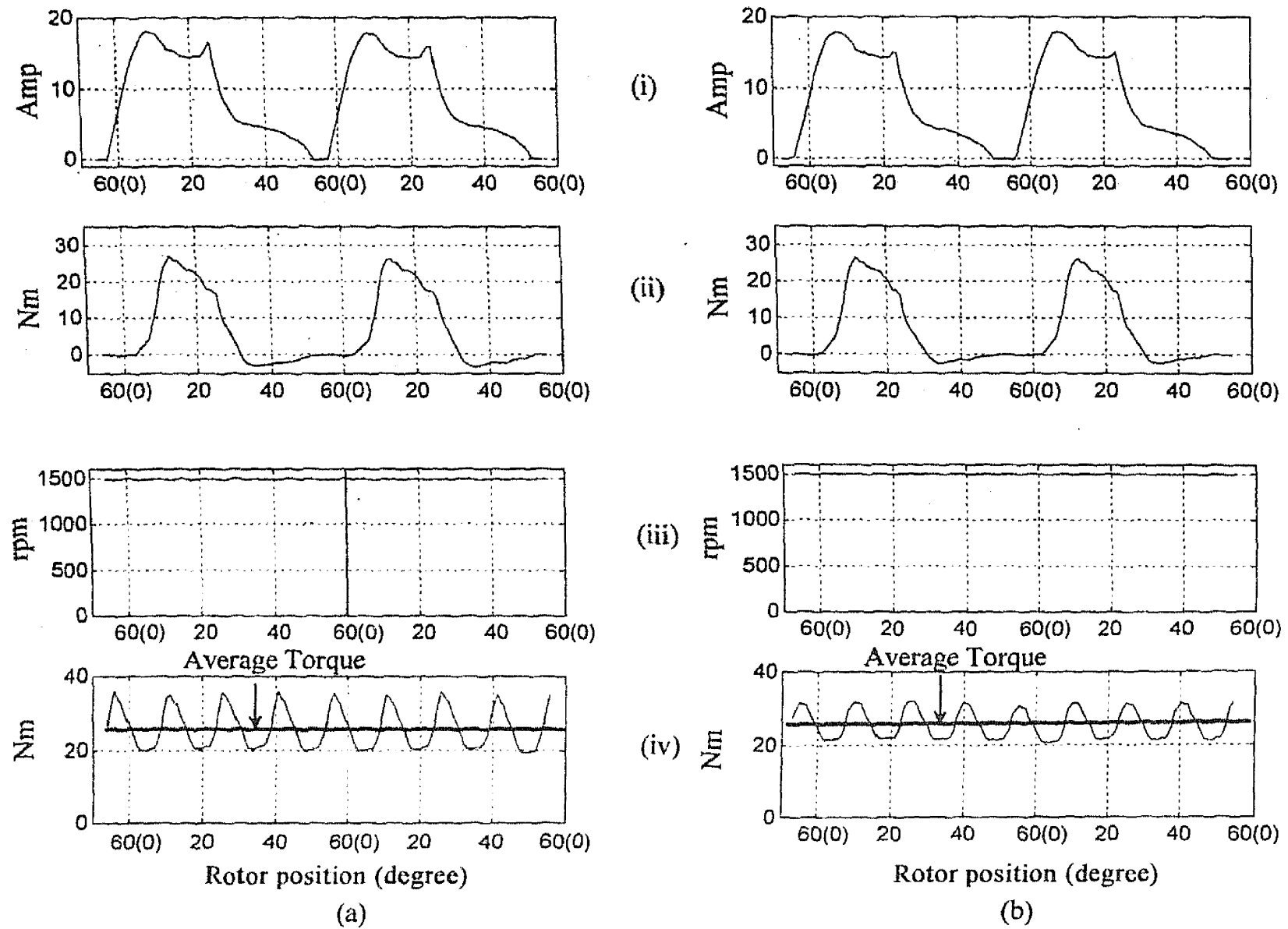
Fig. 10. Comparsion of simulation results of (i) phase current, (ii) phase torque, (iii) speed waveform, (iv) instantaneous and average torque at 1500 rpm and full load (25.5 Nm) for two cases, (a) with $T_{ON} = -5°$ and $T_{OFF} = 23.75°$ and (b) with $T_{ON} = -5.25°$ and $T_{OFF} = 22.5°$.

In simulation, the total control regime is divided in two: low-speed chopping control and high-speed angle control. In the low-speed range (0–900 rpm), the T_{ON} and T_{OFF} angles are functions of speed only as given in Figs 11a and b, respectively. Current is controlled depend ing upon the demand of load. The torque-to-current function generator in the controller makes use of the curves in Fig. 12 for this purpose. These function generators are obtained through simulation and it is shown that current reference is a strong function of torque and it does not vary much with speed. The current references for intermediate values of speeds are
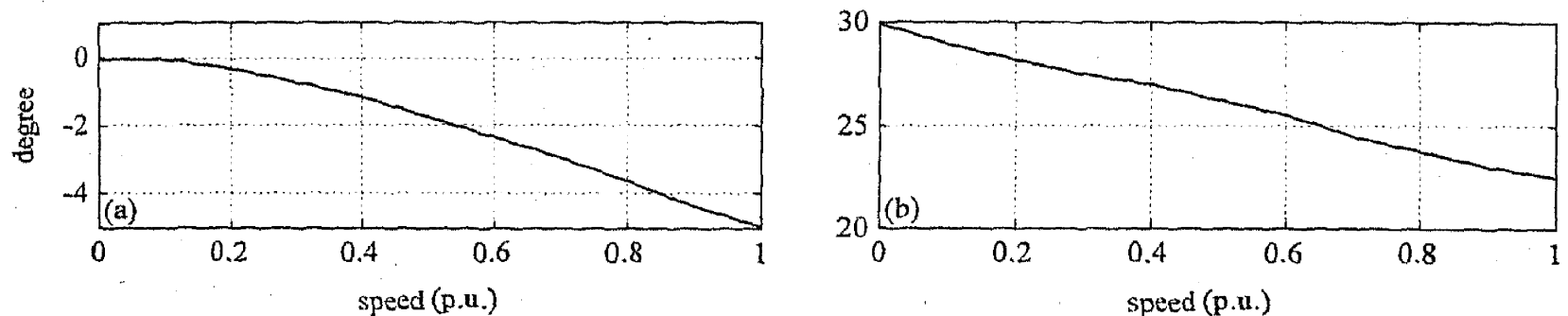

Fig. 11. Variation of T_{ON} and T_{OFF} angles with speed to obtain maximum torque with a peak current limit of 18 A, (a) T_{ON} vs speed and (b) T_{OFF} vs speed.
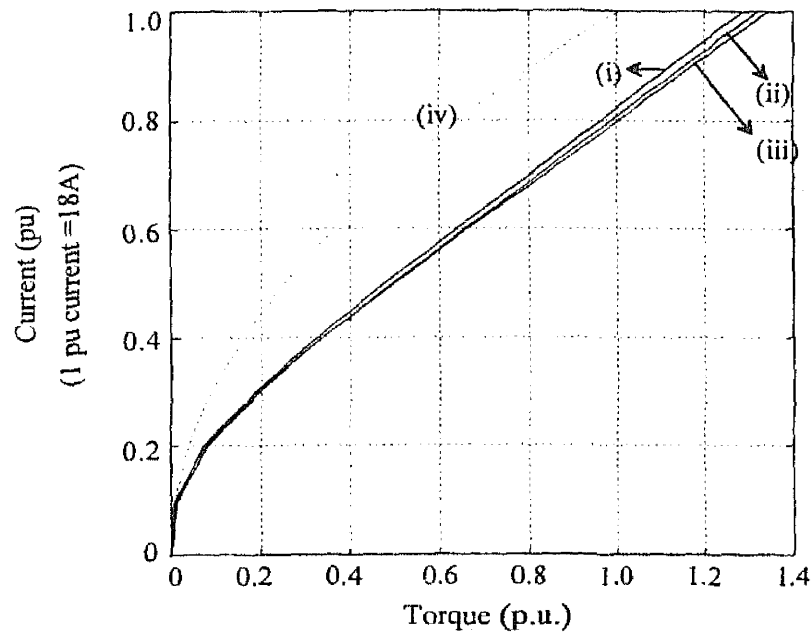
FIG. 12. Current vs torque relationship at different loads and speeds; (i) 900 (ii) 600, (iii) 150, (iv) general square root (I = sqrt(Torque)) relationship for all speeds below 900 rpm (dotted lines)
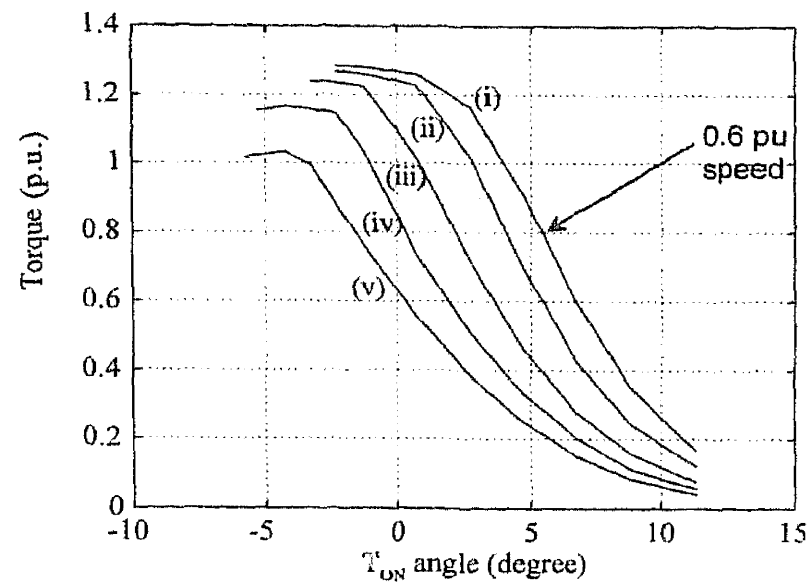
FIG. 13. Torque vs T_{ON} angles at (i) 0.6, (ii) 0.7, (iii) 0.8, (iv) 0.9 and (v) 1.0 pu speeds with peak phase current limit of 18 A.

obtained through linear interpolation. A linearised function of current as the square root of torque is also sxhown in Fig. 12 (iv). Obviously, with this linear relationship, the performance of the drive during transient will be poor compared to what is obtained with function generators. Thus, in the speed range of 0–900 rpm, the main control is realised through hysteresis controller and the T_{ON} and T_{OFF} angles are obtained from look-up tables given in Figs 11a and b, respectively.

In the region 900–1500 rpm, current (torque) is controlled only by angle. The T_{OFF} angles for this speed range are the same as given in Fig. 11b. But the T_{ON} angle varies with both speed and load and the corresponding values for this speed range are plotted in Figs 13 and 14.

Through simulation it is found that for very high-speed operations (2.5–5 pu speed), the T_{ON} angles may be pushed back to $-16°$ and T_{OFF} angle may be advanced up to $+14°$ to obtain better torque speed characteristics. In this speed range, the T_{ON} angles are linearly varied from $-16°$ to $-3.75°$ and the T_{OFF} angles from $+14°$ to $+22.5°$.

Once these parameters are finalised for all the speed and torque conditions, they are stored in a look-up table and referred by the controller. The simulation is carried out using these values for variable speed and load conditions. A PI controller is used for controlling the speed of the motor. A hysteresis controller with maximum switching frequency limitation of 10 kHz is used for current controller.

4.2.3. Results

The torque and speed waveforms at different steady-state and transient operating conditions are presented in Fig. 15. The torque-speed envelope is an important criterion for any electric drive. Figure 16 gives the torque-speed envelope of the SR motor up to base speed (1 pu). It may be noticed that up to the base speed, the SR motor is capable of providing rated torque. At low speeds, with the rated phase currents (18 A for the test motor), the motor is even capable of producing 30% to 35% more than rated torque. At higher speeds, up to 2.5 times the base
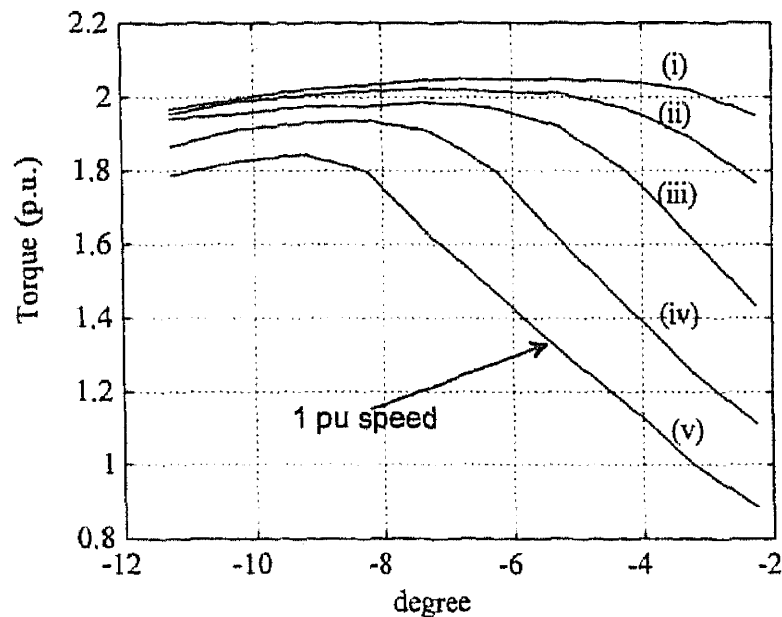
Fig. 14. Torque vs T_{ON} angles at (i) 0.6, (ii) 0.7, (iii) 0.8, (iv) 0.9 and (v) 1.0 pu speeds with 27 A as peak current limit (50% more than rated current).
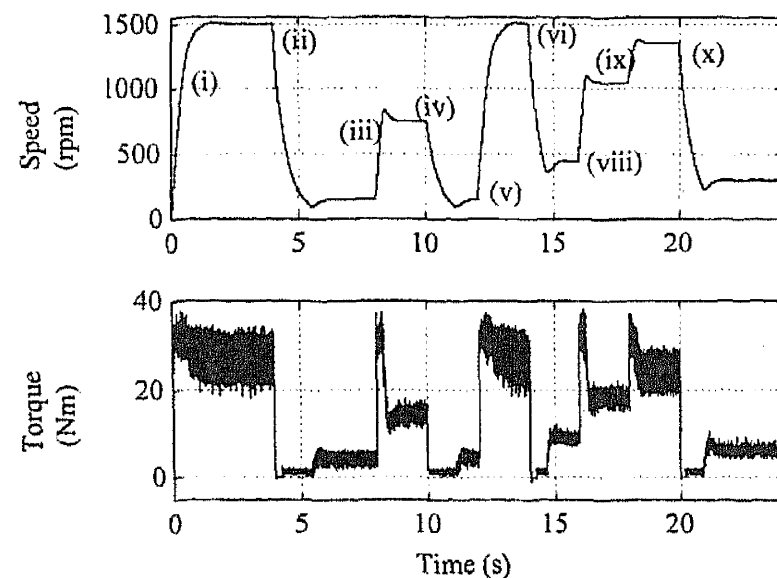
Fig. 15. Speed and torque waveforms during steady-state and different transients of speed. (i)–(x) represent different transients in speed (here load is a function of speed.)

speed, the motor can be operated in constant power mode. Beyond 2.5 pu speed, power falls with the speed. The torque- and power-speed envelopes from 1 to 5 pu speed are presented in Figs 17a and b, respectively.

5. Conclusion

In this paper, modelling and simulation of the SR motor are illustrated. Modelling of the motor is done from the measured flux-linkage characteristics. The model of the mechanical subsystem is obtained by measuring the frictional coefficient and inertia through no load and retardation tests, respectively.

Dynamic simulation of the SR motor with the above model is obtained through time-step integration method. Simulation results of phase current, phase torque, average torque and speed are presented for various operating conditions. Suitable control parameters like T_{ON} and T_{OFF} angles and current reference I^* are obtained from simulation for various operating points. It is shown that for a particular speed and load, different combination of parameters are possible. By choosing suitable values for these parameters it is possible to reduce the torque ripple
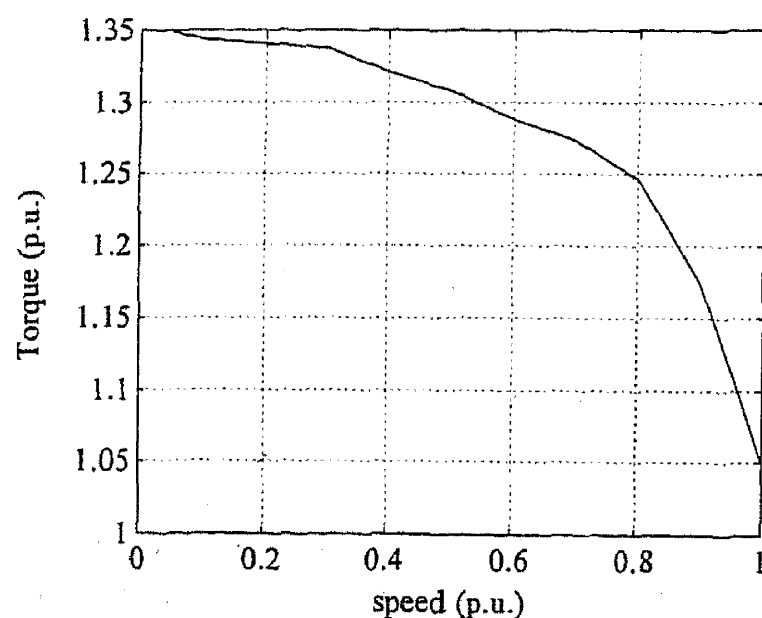

Fig. 16. Torque-speed envelope for less than rated speed (0 to 1 pu speed) with a peak current limit of 18 A.
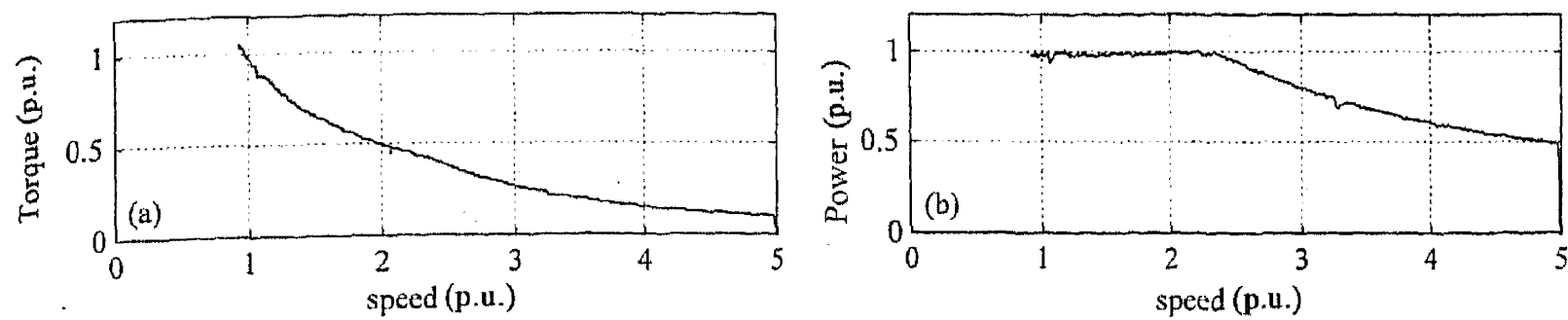
FIG. 17(a). Torque- and (b) power-speed envelopes at more than rated speed (1 to 5 pu).

of the SR motor. In this work, the above parameters are selected based on the criterion of maximising the torque per peak ampere of the SR motor.

The transient performance of the SR motor drive is studied through a closed loop simulation. Speed and torque waveforms during steady state and transient are presented for various operating points. A PI controller is employed for realising the speed controller. It is observed that with the given inertia (0.08 kgm^2) and frictional coefficient (0.0065 Nm/rad/s), the drive using SR motor can reach from zero speed to the rated speed in 1.5 s with a peak current limitation of 18 A.

The torque-speed envelope throughout the operating region is found through simulation. It is seen that the SR motor is capable of following the characteristics of a DC motor. In addition, at lower speeds, 30%–35% more than its rated torque can be achieved with the same peak current. Besides, it is observed that at 50% more than the rated current, the motor can deliver more than twice the rated torque.

References

1. LAWRENSON, P. J., STEPHENSON, J. M., BLENKINSOP, P. T., CORDA, J. AND FULTON, N. N.

   Variable-speed switched reluctance motors, *IEE Proc. B*, 1980, **127**, 253–265.

2. RAMANARAYANAN, V., VENKATESHA, L. AND DEBIPRASAD PANDA

   Flux-linkage characteristics of switched reluctance motor, *Power Electronics Drives and Energy System Conf.* (PEDES-96), New Delhi, India, December 1996, pp. 281–285.

3. MOREIRA, J. C.

   Torque ripple minimisation in switched reluctance motors via bi-cubic spline interpolation, *IEEE-PESC Conf. Rec.*, 1992, pp. 851–856.

4. RAY, W. F. AND BAHADLY, I. H.

   Sensorless methods for determining the rotor position of switched reluctance motor, *Proc. 5th Eur. Conf. on Power Electronics and Applications*, Sept. 13-16, 1993, Vol. 6, IEE publication No. 377, pp. 7–13.

5. DEBIPRASAD PANDA AND RAMANARAYANAN, V.

   Mutual inductance and its effect on steady-state performance and position estimation method of switched reluctance motor drive, *Proc. IEEE, IAS Annual Meeting*, Oct. 1999, Phoenix, USA, pp. 2227–2234.

6. DEBIPRASAD PANDA AND RAMANARAYANAN, V.

   An accurate position estimation of switched reluctance motor with smooth starting, *Proc. IEEE Int. Conf. on Industrial Technology* (ICIT), Jan. 2000, Goa, India.

7. DEBIPRASAD PANDA AND RAMANARAYANAN, V.

   A novel sensorless method with self-measured flux-linkage characteristics, *Proc. IEEE Power Electronics Specialist Conf.* (PESC 2000), Galway, Ireland, pp. 1569–1574.

8. POLLOCK, C. AND WU, C. Y.   Acoustic noise cancellation techniques for switched reluctance drives, *IEEE IAS Conf. Proc.*, 1995, pp. 448–455.

9. DEBIPRASAD PANDA AND   A composite control strategy for low-noise and sensorless operation
   RAMANARAYANAN, V.   of switched reluctance motor, *Proc. IEEE IAS Annual Meeting*, 2000, Rome, Italy, pp. 1751–1758.

10. MILLER, T. J. E.   *Switched reluctance motors and their control*, Magna Physics Publishing and Clarendon Press, 1993.

11. ARUMUGAM, R., LOWTHER, D. A.,   Magnetic field analysis of switched reluctance motor using a two-
    KRISHNAN, R. AND LINDSAY, J. F.   dimensional finitie element model, *IEEE Trans.*, 1985, **MAG-21**, 1883–1885.